Electronic Supporting Information

Defect engineering of UiO-66 for CO_2 and H_2O uptake – a combined experimental and simulation study

Weibin Liang,[a] Campbell J. Coghlan,[b] Florence Ragon,[a] Marta Rubio-Martinez,[c] Cameron J. Kepert,[a] Deanna M. D'Alessandro,[a*] and Ravichandar Babarao[c*]

[a]School of Chemistry, University of Sydney, Australia
[b]Centre for Advanced Nanomaterials, School of Chemistry & Physics, The University of Adelaide, Adelaide, Australia
[c] CSIRO Manufacturing, Private Bag 33, Clayton South MIDS, Victoria 3169, Australia

*Corresponding author emails: deanna.dalessandro@sydney.edu.au and ravichandar.babarao@csiro.au

S1 Syntheses

All chemicals and solvents were purchased from commercial sources and used as received without further purification.

S1.1 Conventional solvothermal synthesis of perfect UiO-66

3.78 g of $ZrCl_4$, 2.8 mL 35% HCl and 5.39 g of 1,4-benzenedicarboxylic acid (BDC) were dissolved in 98 mL of dimethylformamide (DMF). The synthesis mixture was stirred until the solution was completely transparent and then transferred to a Teflon liner and sealed in stainless steel autoclave where it was heated at 220 °C for 20 hours. After cooling down to room temperature, the solid was centrifuged and immersed in DMF at 100 °C for 150 minutes. The product was dried overnight at 60 °C. The same procedure was repeated again. Subsequently a methanol exchange was performed at 100 °C for 24 hours using an extractor thimbles. The final product was dried in vacuum at 60 °C.

S1.2 Microwave-assisted d-UiO-66-aC syntheses (a = 05, 1, or 2, volume of additives used in the MOFs synthesis protocol; C = HCl or FA, HCl = concentrated hydrochloric acid; FA = formic acid)

Microwave syntheses of d-UiO-66-aCs were conducted using an Anton Paar Monowave 300 microwave oven. A 30 mL glass microwave vial was charged with 1 mmol $ZrCl_4$ (>99.9%, Sigma-Aldrich) and 1 mmol 1,4-benzenedicarboxylic acid (H_2bdc, 98%, Sigma-Aldrich). Thereafter, concentrated hydrochloric acid (conc. HCl, 37%, Merck) or formic acid (reagent grade, ⩾ 95%, Sigma-Aldrich) and *N,N´*-dimethylformamide (DMF, Ajax) were introduced. The mixture was heated with magnetic stirring to 180 °C within 2 min, and held at this temperature for 90 min before cooling to 55 °C within 2 min. The precipitates were vacuum filtered, and repeatedly washed with DMF and ethanol. The resulting powder was dried in vacuum. A summary of the reaction conditions is provided in Table S1.

Table S1 Synthesis conditions for the d-UiO-66-aCs using microwave heating.

Phase[a]	$ZrCl_4$ 1	H_2bdc 1	DMF [mL]	conc. HCl [mL]	Formic acid [mL]	H_2O [mL][c]	T [ºC][d]	Time [min]
1-05HCl	1	1	6	0.5	0	0	180	90
1-1HCl	1	1	6	1	0	0	180	90
1-2HCl	1	1	6	2	0	0	180	90
1-05FA	1	1	6	0	0.5	0.2	180	90
1-1FA	1	1	6	0	1	0.2	180	90
1-2FA	1	1	6	0	2	0.2	180	90

[a]1 = d-UiO-66; [b]H_2bdc = 1,4-benzenedicarboxylic acid; [c]for d-UiO-66-aFAs, addition of H_2O is crucial for pure UiO-66 phase, without which polymorphous MIL-140A phase appeared even at low synthesis temperature (140 °C); [d]microwave heating, temperature ramp to 180 ºC within 2 min.

S2 X-ray powder diffraction (XRPD)

XRPD measurements were performed on a PANalytical X'pert Pro diffractometer fitted with a solid-state PIXcel detector (45 kV, 40 mA, 1° divergence and anti-scatter slits, and 0.3 mm receiver and detector slits) using Cu-Kα (λ = 1.5406 Å) radiation. Profile fits were performed using the *Le Bail* extraction method in GSAS.[7]

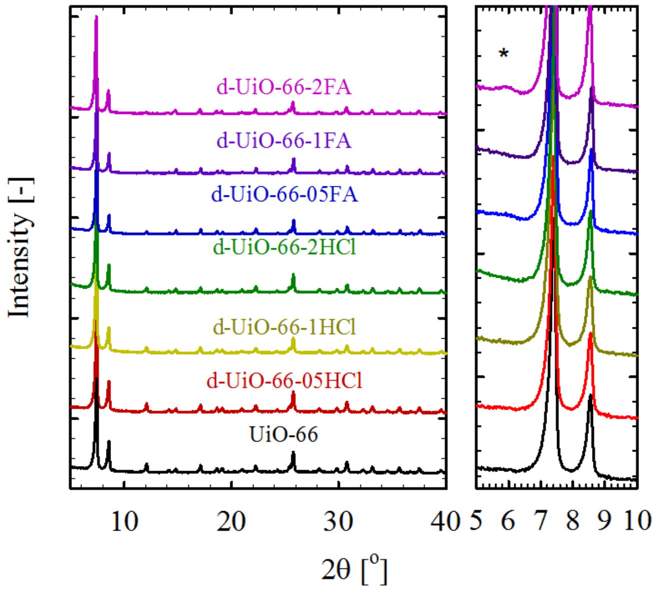

Figure S1 Full (5 – 40 °, left) and low-angle (5 – 10 °, right) XRPD spectra for d-UiO-66-aC (a = 05, 1, or 2, volume of additives used in the MOFs synthesis protocol; C = HCl or FA, HCl = concentrated hydrochloric acid; FA = formic acid), type of additives used in the MOFs synthesis protocol). The asterisks in the additional low-angle peak region for d-UiO-66-2FA represent the *reo* type defects.

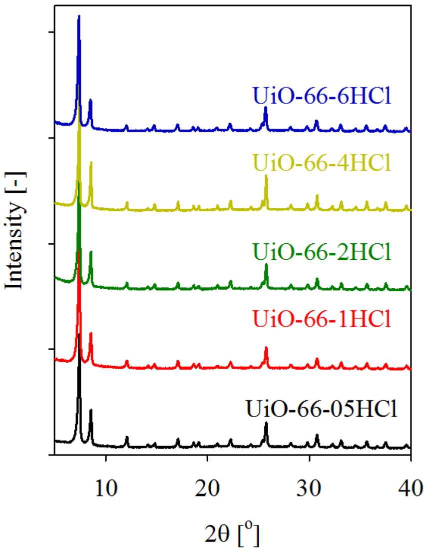

Figure S2 XRPD patterns of activated d-UiO-66-05HCl, d-UiO-66-1HCl, d-UiO-66-2HCl, d-UiO-66-4HCl, and d-UiO-66-6HCl.

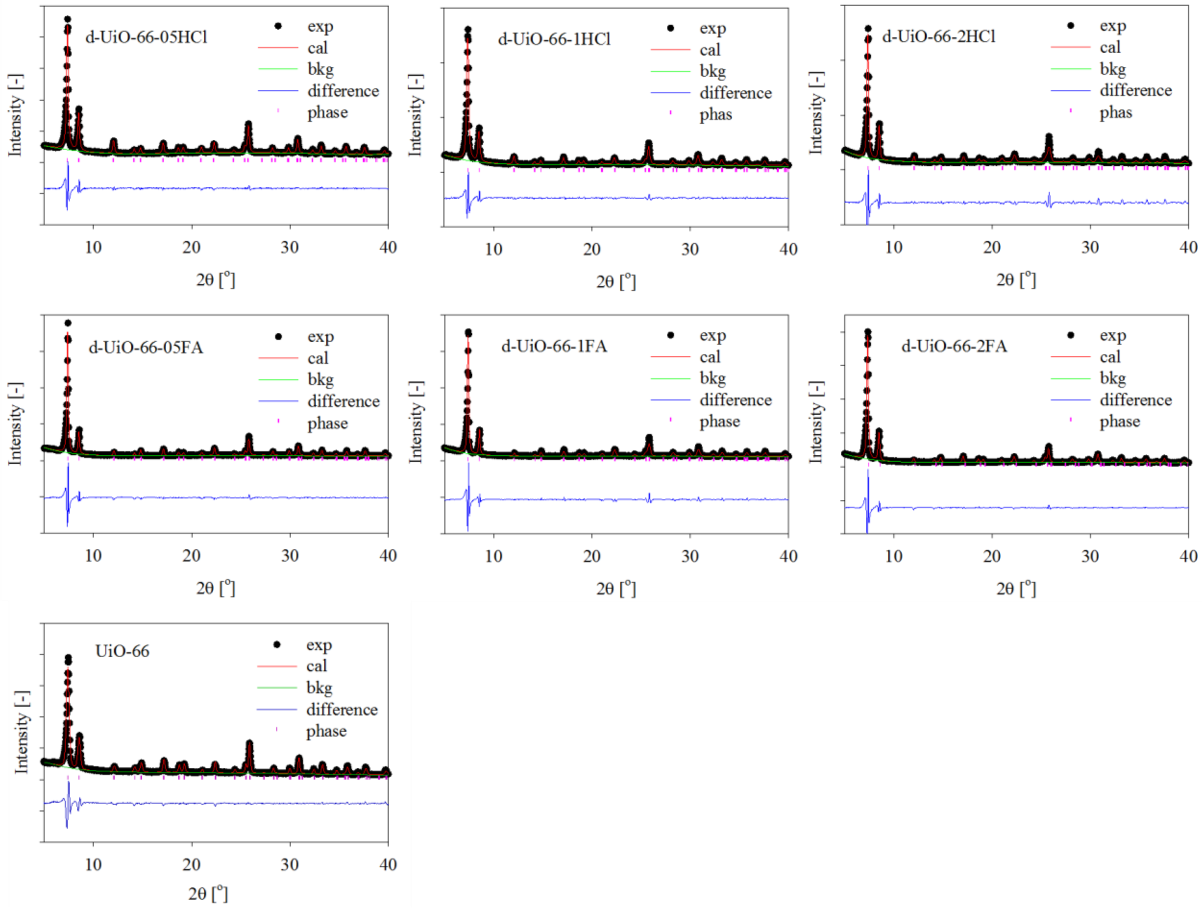

Figure S3 *Le Bail* refinements of d-UiO-66-05HCl, d-UiO-66-1HCl, d-UiO-66-2HCl, d-UiO-66-05FA, d-UiO-66-1FA, d-UiO-66-2FA, and UiO-66 showing the experimental (black), refined (red), and difference (blue) patterns. The positions of the Bragg peaks are indicated by the pink bars.

Table S2 Simulated *Le Bail* cell parameters for d-UiO-66-05HCl, d-UiO-66-1HCl, d-UiO-66-2HCl, d-UiO-66-05FA, d-UiO-66-1FA, and d-UiO-66-2FA .

Phase	Space group	Cell parameter	Volume
		a [Å]	[Å^3]
UiO-66	*F m -3 m*	20.63(1)	8785.80(1)
d-UiO-66-05HCl	*F m -3 m*	20.77(1)	8961.33(2)
d-UiO-66-1HCl	*F m -3 m*	20.71(1)	8888.76(2)
d-UiO-66-2HCl	*F m -3 m*	20.70(1)	8876.65(3)
d-UiO-66-05FA	*F m -3 m*	20.68(1)	8848.41(2)
d-UiO-66-1FA	*F m -3 m*	20.69(1)	8858.84(3)
d-UiO-66-2FA	*F m -3 m*	20.56(1)	8700.04(2)

In previous studies, UiO-66 (Hf or Zr) materials with ordered missing linker defects manifested characteristic symmetry forbidden reflections (indexing to the (100) and (110) peaks of the primitive cell) in the low angle region of their XRPD patterns (4-6°).[2, 3] In the present study, except for d-UiO-66-2FA, such weak and broad symmetry forbidden peaks were not observed, probably due to the high conc. HCl dosage used in the synthesis protocol, resulting in randomised rather than ordered defect-nano-regions (*vide infra*).

S3 Chemical formula determination for d-UiO-66-aC

S3.1 Thermogravimetric analysis

TGA measurements were carried out on a DISCOVERY TGA Thermogravimetric Analyzer. Approximately 5 mg of sample was placed on a platinum pan which was heated under a flow of air at a rate of 5 °C.min^{-1} up to 700 °C

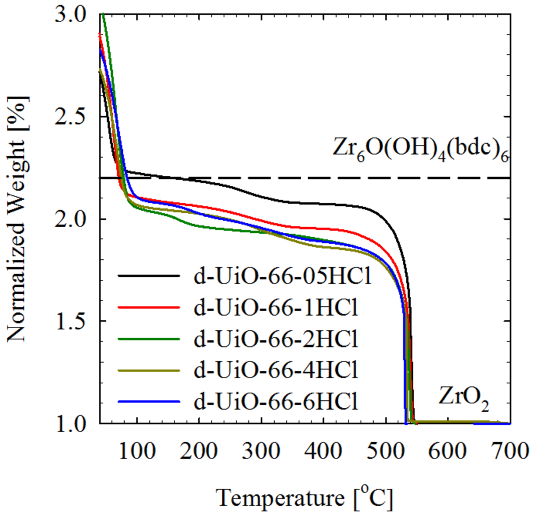

Figure S4 Thermogravimetric analysis (TGA) showing the weight loss (relative to ZrO_2) for d-UiO-66-05HCl, d-UiO-66-1HCl, d-UiO-66-2HCl, d-UiO-66-4HCl, and d-UiO-66-6HCl. Dashed lines indicate the theoretical weight (relative to ZrO_2) for UiO-66.

S3.2 Scanning electron microscopy-energy dispersive spectroscopy (SEM-EDS)

Field-emission SEM (FE-SEM) images and EDS spectra were obtained using a Zeiss ULTRA plus microscope (working distance 9 mm; acceleration voltage 20 kV). Samples were prepared by dispersing the powdered solids in ethanol to produce a suspension that was deposited onto a carbon block and dried in air. EDS results are calculated as an average of at least 9 different areas of a samples.

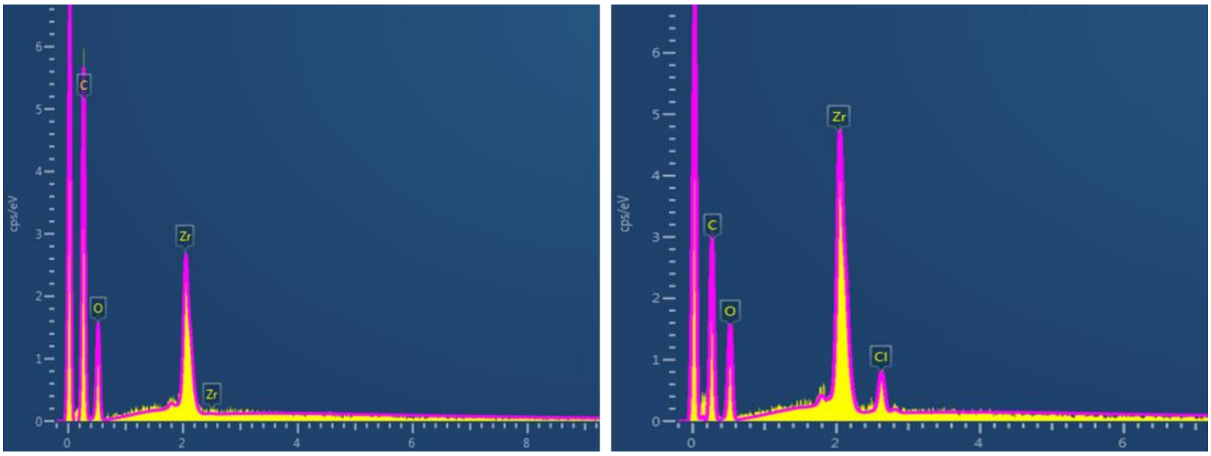

Figure S5 Examples of raw EDS spectra: UiO-66 (left) and d-UiO-66-05FA (right).

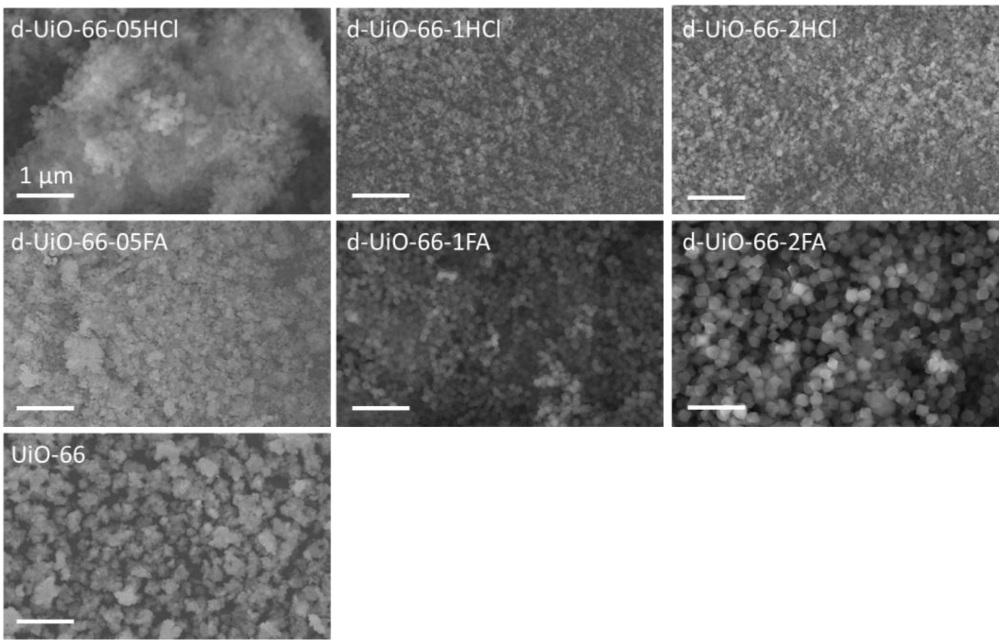

Figure S6 SEM images of d-UiO-66-aCs and UiO-66. The scale bar represents 1 µm for all SEM images.

S3.3 Nuclear magnetic resonance (NMR)

^{1}H NMR spectra were recorded in deuterated solvents using a Bruker AVANCE200 NMR Spectrometer. The d-UiO-66-aCs (~20 mg) sample was digested in KOH/D_2O. The actual molecular ratio between formate and 1,4-benzenedicarboxylate was calculated by integrating the proton signals of the ligands in the ^{1}H NMR spectra.

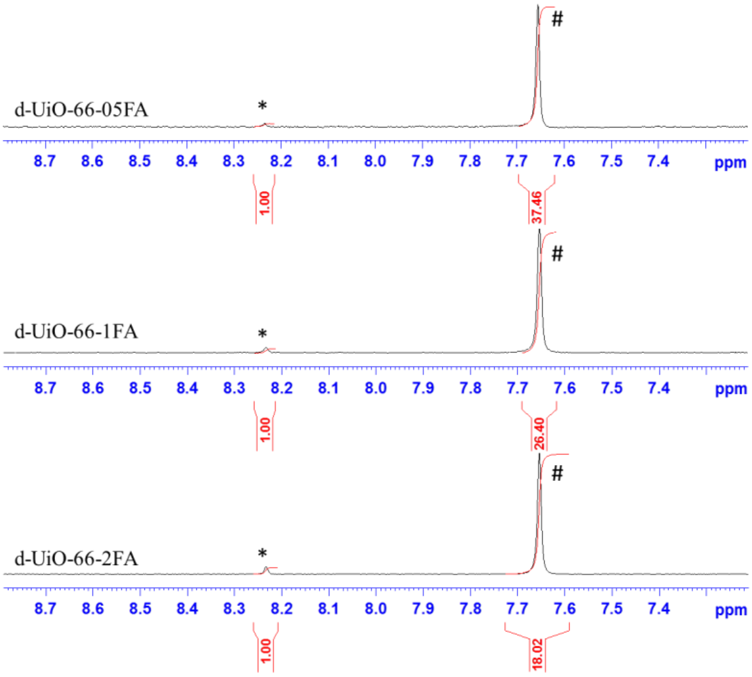

Figure S7 Examples of ^{1}H NMR spectra of alkaline-digested (KOH/D_2O) d-UiO-66-aFA (a = 05, 1, and 2). Asterisk (*) indicates the proton signal of formate and hash mask (#) of 1,4-benzenedicarboxylate.

S3.4 Chemical formula determination for d-UiO-66-aCs

The presence of structural defects was evidenced by the aerobic decomposition of d-UiO-66-aC in TGA analysis. As shown in Figure 1b and S8, the TGA traces of all samples can be deconvoluted into three distinguished stages: solvent volatilization (~100 °C), compensating-agent elimination (250–350 °C), and framework decomposition (500–550 °C) (Figure 1b). Considering the chemical equation for perfect UiO-66(Zr), the molecular weight of $[Zr_6O_6(bdc)_6]$ (product at 350 °C) is a factor of 2.2 higher than six ZrO_2 (only solid product at 700 °C).[3] The concentration of the missing-linker defects can be addressed by comparison of the TGA plateau at 350 °C (solvent-free and dehydrated materials) and the end weight at 700 °C (ZrO_2).[3, 4] In addition, incorporation of formate, chloride and/or hydroxide anions to the $[Zr_6O_4(OH)_4]^{12+}$ cluster to compensate for linker deficiencies proved to be feasible both experimentally and theoretically.[5, 6] Although direct incorporation of Cl^- within the Zr-oxo cluster by replacing the -OH group, forming $[Zr_6O_4Cl(OH)_3]^{12+}$, is plausible at low synthesis temperatures,[3] such a phenomenon is thermodynamically unfavorable in our case ($T_{synthesis}$ = 180 °C).[7] Thus, we just consider peripheral coordination of Cl^-, $HCOO^-$ and OH^- in the d-UiO-66 formula calculation.

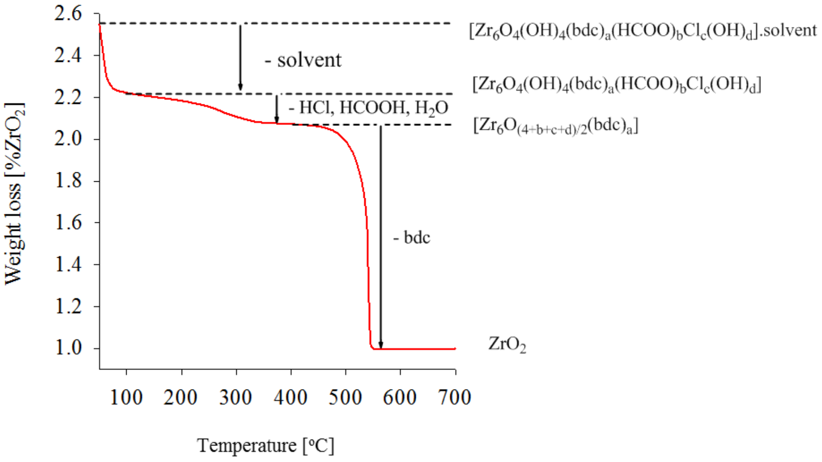

Figure S8 Illustration of TGA patterns of UiO-66(Zr) shows three steps corresponding to, in turn, solvent volatilization (~100 °C), compensating-agent elimination (250–350 °C), and framework decomposition (500–550 °C).

The aerobic decomposition d-UiO-66-aCs can be expressed as the following equation:

$$[Zr_6O_4(OH)_4(bdc)_a(HCOO)_bCl_c(OH)_d] \xrightarrow{350\ ^\circ C, O_2} [Zr_6O_{\frac{12+b+c+d}{2}}(bdc)_a] + bHCOOH + cHCl + \frac{4-b-c+d}{2}H_2O$$

where a, b, c, and d can be calculated via k_a, k_b, and k_c measured from TGA, ^{1}H NMR and EDS, respectively.

Values of k_a, molecular weight between UiO-66 (solvent free and dehydrated) and ZrO_2, were extracted from the nomalised aerobic TGA data (Figure 1b).

$$k_a \equiv \frac{[Zr_6O_{\frac{12+b+c+d}{2}}(bdc)_a]}{6ZrO_2} = \frac{547.344 + 16 \times \left(\frac{12+b+c+d}{2}\right) + 164.113 \times a)}{6 \times 123.218}$$

The molecular ratios between formate and 1,4-benzenedicarboxylate (k_b) in the d-UiO-66-aCs were quantified by taking ^{1}H NMR spectra of the alkaline (KOH/D_2O) digested MOFs.

$$k_b \equiv \frac{M_{formate}}{M_{bdc}} = \frac{b}{a}$$

The atomic ratios between chloride and zirconium in d-UiO-66-aCs were measured by SEM-EDS analysis.

$$k_c \equiv \frac{A_{Cl}}{A_{Zr}} = \frac{c}{6}$$

A summary table for k_a, k_b and k_c is provided in Table S3. The actual values of a, b, c and d were calculated *via* solving the following equations using Excel (Microsoft Corporation).

$$\begin{cases} k_a \equiv \dfrac{547.344 + 16 \times \left(\dfrac{12+b+c+d}{2}\right) + 164.113 \times a)}{6 \times 123.218} \\ k_b \equiv \dfrac{b}{a} \\ k_c \equiv \dfrac{c}{6} \\ a+b+c+d = 12 \end{cases}$$

Table S3 Summary table for k_a, k_b and k_c.

Sample	TGA plateau @ 350 °C (k_a)[a]	$M_{formate}/M_{bdc}$ (k_b)[b]	A_{Cl}/A_{Zr} (k_c)[c]
UiO-66[d]	2.20	0	0
d-UiO-66-05HCl	2.08	0	0.11
d-UiO-66-1HCl	1.96	0	0.18
d-UiO-66-2HCl	1.92	0	0.28
d-UiO-66-05FA	1.98	0.11	0.19
d-UiO-66-1FA	1.94	0.15	0.14
d-UiO-66-2FA	1.89	0.22	0.10

[a]data was taken from normalised aerobic TGA data; [b]molecular ratio between formate and 1,4-benenedicarboxylate was quantified by taking ^{1}H NMR spectra of the alkaline (KOH/D_2O) digested MOFs; [c]data was obtained from EDS analysis; [d]the chemical formula for UiO-66 is calculated using the same method as other defective UiO-66 samples.

A summary table for the calculated formula of UiO-66 and d-UiO-66-aCs is provided in Table S4.

Table S4 Calculated formula of d-UiO-66-aCs.

Compound	Formula
UiO-66	$[Zr_6O_4(OH)_4(bdc)_{6.0}]$
d-UiO-66-05HCl	$[Zr_6O_4(OH)_4(bdc)_{5.4}Cl_{0.7}(OH)_{0.5}]$
d-UiO-66-1HCl	$[Zr_6O_4(OH)_4(bdc)_{4.8}Cl_{1.1}(OH)_{1.3}]$
d-UiO-66-2HCl	$[Zr_6O_4(OH)_4(bdc)_{4.6}Cl_{1.7}(OH)_{1.1}]$
d-UiO-66-05FA	$[Zr_6O_4(OH)_4(bdc)_{4.9}(HCOO)_{0.5}Cl_{1.2}(OH)_{0.5}]$
d-UiO-66-1FA	$[Zr_6O_4(OH)_4(bdc)_{4.7}(HCOO)_{0.7}Cl_{0.8}(OH)_{1.1}]$
d-UiO-66-2FA	$[Zr_6O_4(OH)_4(bdc)_{4.5}(HCOO)_{1.0}Cl_{0.6}(OH)_{1.5}]$

S4 Adsorption analysis

S4.1 N_2 adsorption at 77 K and CO_2 adsorption under low-pressure (<1 bar)

N_2 sorption isotherms were recorded on a 3Flex Surface Characterisation Analyser (Micromeritics Instruments Inc.). Approximately 100 mg of the powdered solid was loaded into a glass analysis tube and outgassed for 16 h under dynamic vacuum (~10^{-6} bar) at 160 °C. N_2 adsorption and desorption isotherms were measured at 77 K and the surface areas were calculated using the Brunauer–Emmett–Teller (BET)[8] or Langmuir[9] models. CO_2 adsorption and desorption isotherms were measured at 293, 303, and 313 K.

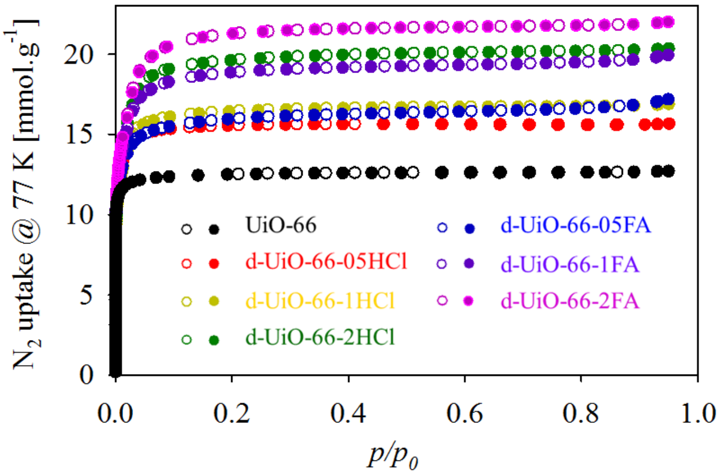

Figure S9 N_2 adsorption (filled circle) and desorption (open circle) isotherms, measured at 77 K.

The pore-size-distribution calculations were carried out using the MicroActive software DFT package (non-local density functional theory calculations, NLDFT, based on the *N_2-Cylindrical Pores – Oxide Surface DFT model* in the MicroActive software package, Micromeritics Instruments Inc.).

Calculation of the CO_2 heat of adsorption involves the generation of an interpolated curve by spline fitting of data points using MicroActive software (version 3.00, Micromeritics Instrument Corporation). This was used to fit data for CO_2 adsorption isotherms at 293, 303, and 313 K to the Clausius–Clapeyron equation, which was used to determine the isosteric enthalpy of adsorption at specific surface coverage.

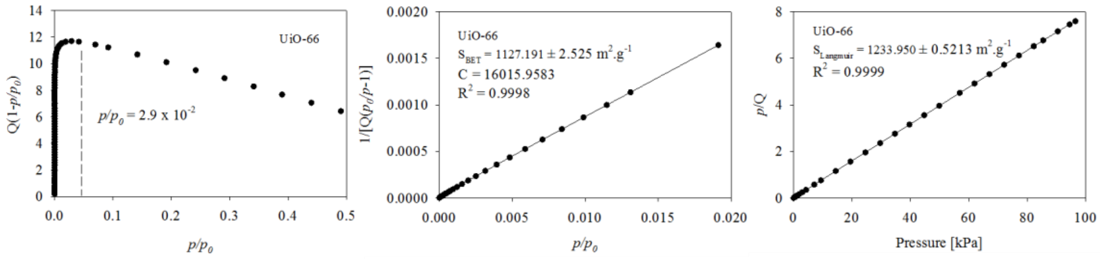

Figure S10 Consistency plot (left), BET fit (middle), and Langmuir fit for UiO-66.

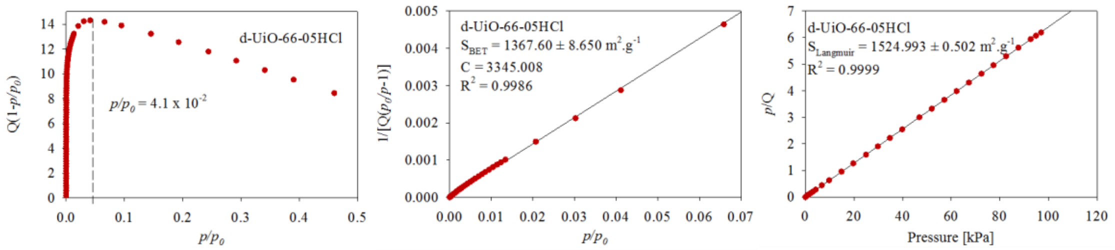

Figure S11 Consistency plot (left), BET fit (middle), and Langmuir fit for d-UiO-66-05HCl.

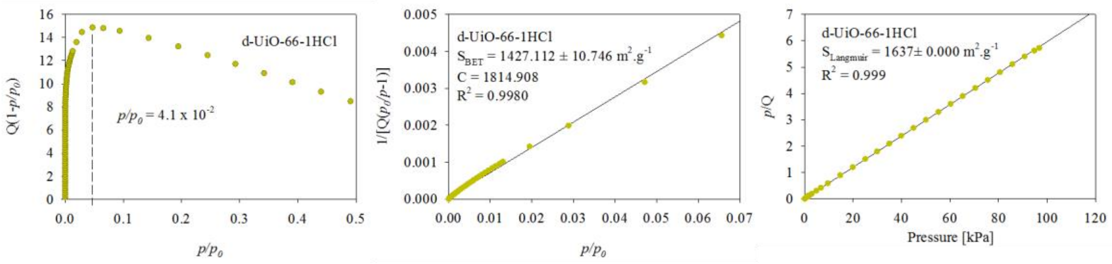

Figure S12 Consistency plot (left), BET fit (middle), and Langmuir fit for d-UiO-66-1HCl.

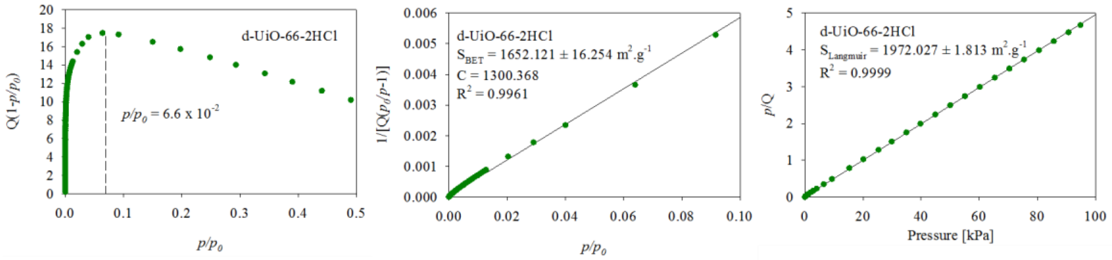

Figure S13 Consistency plot (left), BET fit (middle), and Langmuir fit for d-UiO-66-2HCl.

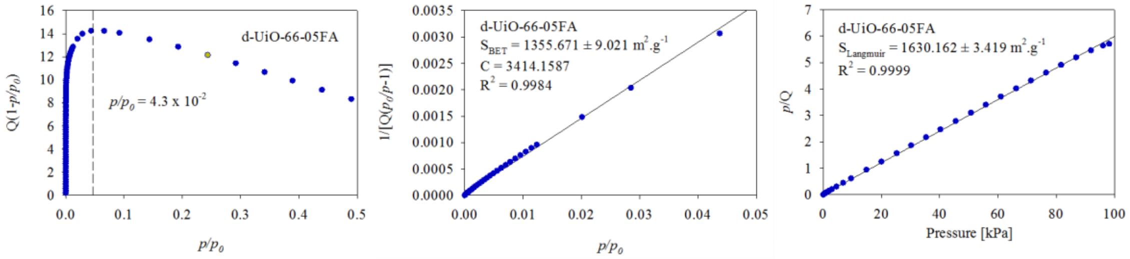

Figure S14 Consistency plot (left), BET fit (middle), and Langmuir fit for d-UiO-66-05FA.

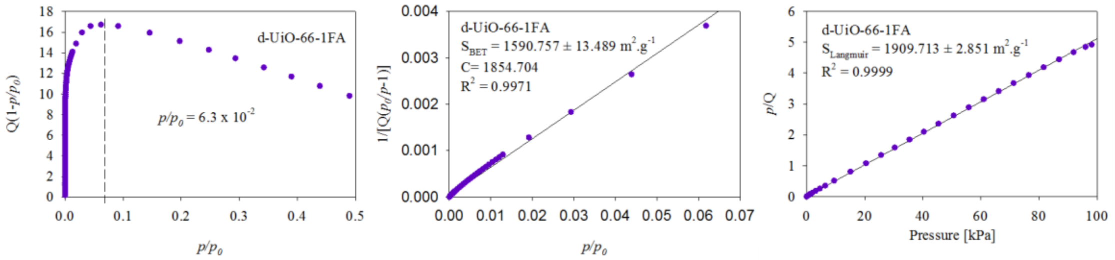

Figure S15 Consistency plot (left), BET fit (middle), and Langmuir fit for d-UiO-66-1FA.

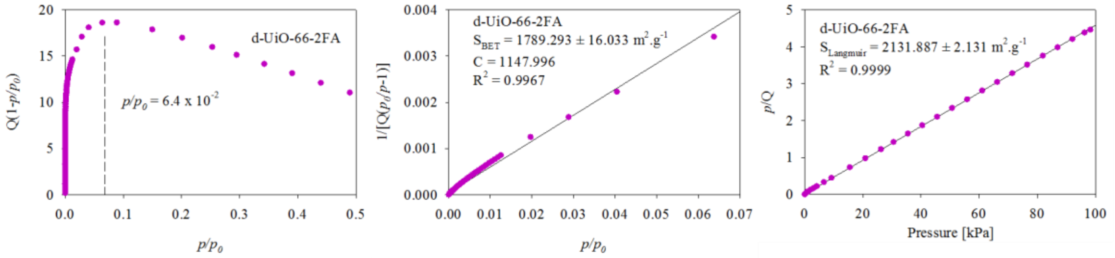

Figure S16 Consistency plot (left), BET fit (middle), and Langmuir fit for d-UiO-66-2FA.

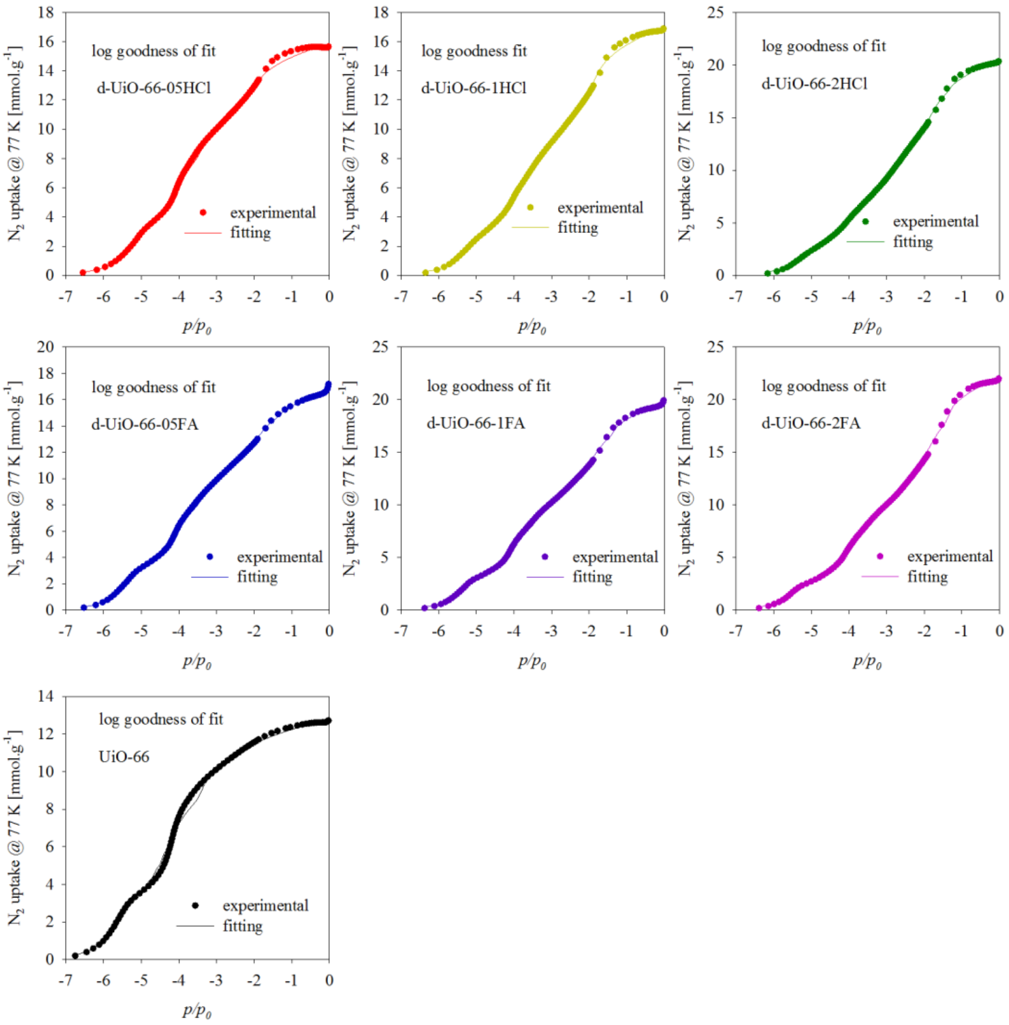

Figure S17 Log goodness of fit plots of N_2 adsorption isotherm for d-UiO-66-05HCl, d-UiO-66-1HCl, d-UiO-66-2HCl, d-UiO-66-05FA, d-UiO-66-1FA, and d-UiO-66-2FA.

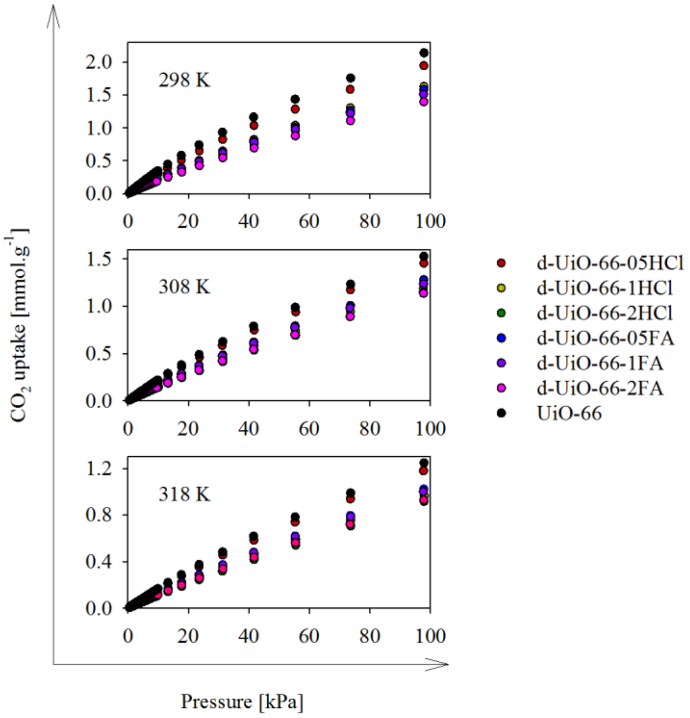

Figure S18 CO_2 adsorption isotherms at 298, 308, and 318 K for UiO-66 and d-UiO-66-aCs.

S4.2 CO_2 adsorption under high-pressure (< 35 bar)

Prior to analysis, samples (~100 mg) were degassed under high vacuum for 24 hours at 160 °C. The high pressure CO_2 experiments were conducted at 298 K up to 35 bar using a high pressure volumetric analyser (Micromeritics HPVA-100).

Table S5 Summary table for the gas adsorption data (BET and Langmuir surface area and pore size and CO_2 adsorption data)

Compound	S_{BET} [$m^2.g^{-1}$]^a	$S_{Langmuir}$ [m2.g-1]^a	V_{total} [$cm^3.g^{-1}$]^b	$d_{pore\ width}$ [Å]^c	$n_{CO2@0.15bar,298K}$ [$mmol.g^{-1}$]	$n_{N2@0.75bar,298K}$ [$mmol.g^{-1}$]	CO_2/N_2 Selectivity^d	$n_{CO2@1bar,298K}$ [$mmol.g^{-1}$]	$n_{CO2@35bar,298K}$ [$cm^3.g^{-1}$]
UiO-66	1127.2(2.5)	1233.9(0.5)	0.44	8.2; 10.9	0.07	0.44	31.43	2.16	207.20
d-UiO-66-05HCl	1376.6(8.7)	1525.0(0.5)	0.54	8.8; 11.2; 15.3	0.16	0.44	13.75	1.97	265.07
d-UiO-66-1HCl	1427.1(10.7)	1638.0(1.2)	0.59	8.8; 11.3; 15.6	0.15	0.34	11.33	1.66	342.39
d-UiO-66-2HCl	1652.1(16.3)	1972.0(1.8)	0.71	8.8; 11.2; 15.6; 18.8	0.16	0.29	9.06	1.61	405.90
d-UiO-66-05FA	1355.7(9.0)	1630.2(3.4)	0.60	8.5; 11.2; 15.6; 18.6	0.05	0.33	33.00	1.61	413.12
d-UiO-66-1FA	1590.8(13.5)	1909.7(2.8)	0.69	8.5; 11.2; 15.7; 18.6	0.06	0.32	26.67	1.54	383.62
d-UiO-66-2FA	1789.3(16.0)	2131.9(2.1)	0.95	8.3; 11.2; 15.7; 18.7	0.06	0.28	23.33	1.42	336.94

[a] calculated from the N_2 adsorption isotherms measured at 77 K. Values in parentheses indicate the uncertainties; [b] calculated from the amount of N_2 at 1 bar at 77 K; c Pore-size distribution for UiO-66 and d-UiO-66-aC extracted from the N_2 adsorption isotherms at 77 K by NLDFT model; [d] co-adsorption selectivity at 299 K, $\alpha_{CO2/N2} = (Q_{CO2,0.15\ bar}/Q_{N2,\ 0.75\ bar})/(p_{CO2}/p_{N2})$; p = 0.15 bar for CO_2 and 0.75 bar for N_2

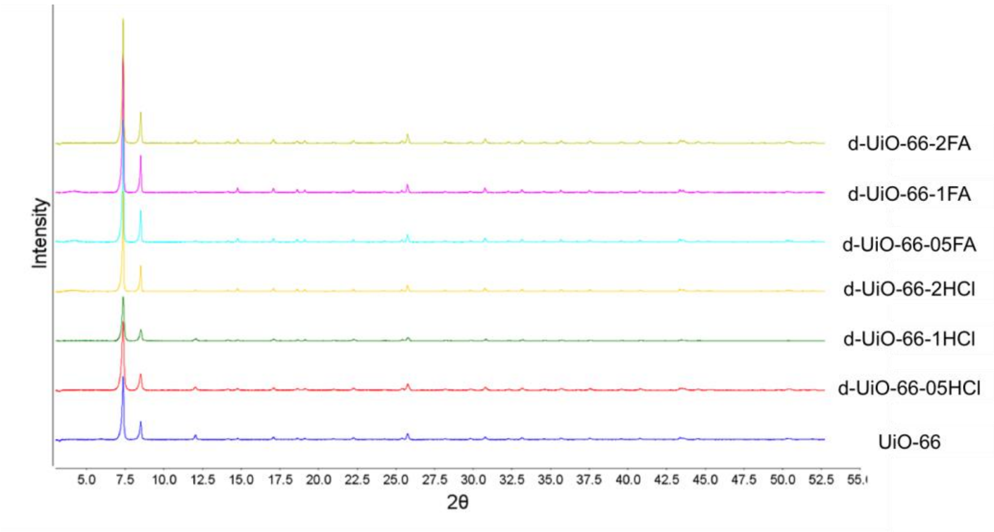

Figure S19 XRPD spectra for d-UiO-66-aC (a = 05, 1, or 2, volume of additives used in the MOFs synthesis protocol; C = HCl or FA, HCl = concentrated hydrochloric acid; FA = formic acid), type of additives used in the MOFs synthesis protocol) and perfect UiO-66 after the high-pressure CO_2 adsorption measurement.

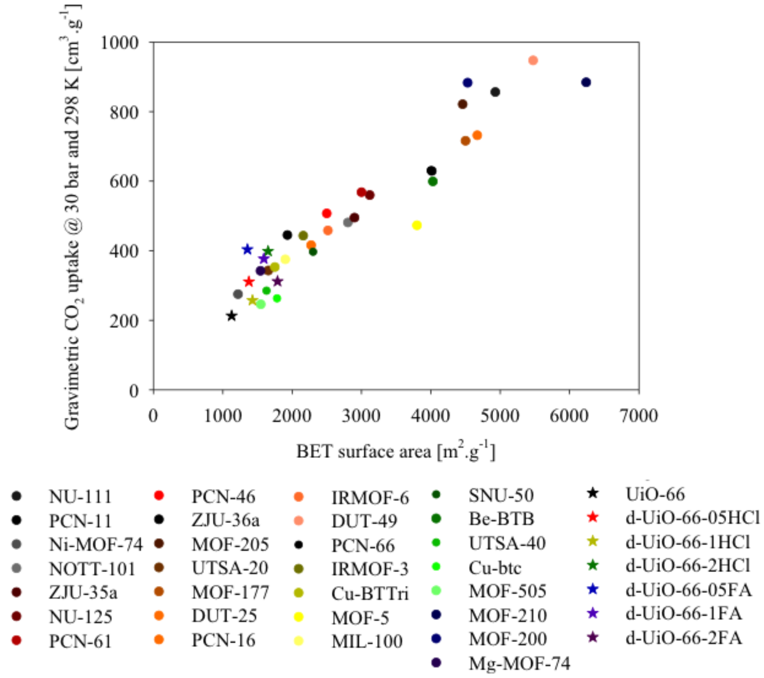

Figure S20 Plots of CO_2 uptake at 298 K and 30 bar *vs.* BET surface area for some reported MOFs and defective UiO-66 materials in this study.[8-23]

S4.3 H_2O adsorption analysis

Water sorption isotherms were performed on a Hiden-Isochema Intelligent Gravimetric Analyser (IGA). Prior to adsorption, the sample was outgassed under vacuum (10^{-5} bar) at 160 °C overnight. Sample was cooled to analysis temperature (25 °C) and the dry mass recorded. The sample chamber was pressurized to a set pressure and allowed to equilibrate for 120 minutes before moving to the next pressure point.

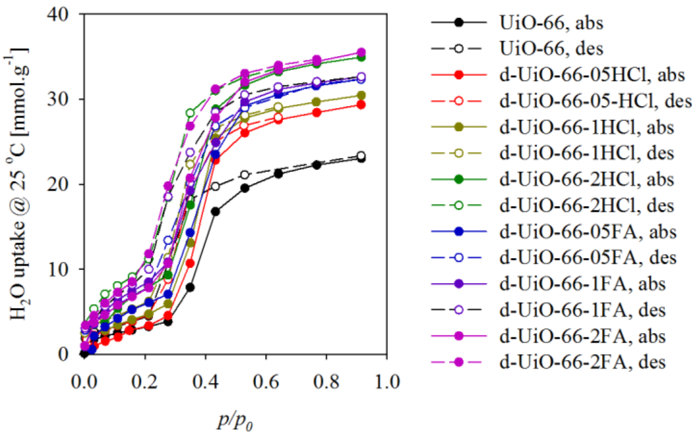

Figure S20 Water adsorption (filled circle) and desorption (open circle) isotherms at 298 K for UiO-66, d-UiO-66-aHCl and d-UiO-66-aFA (a = 05, 1, or 2, volume of additives used in the synthesis protocol).

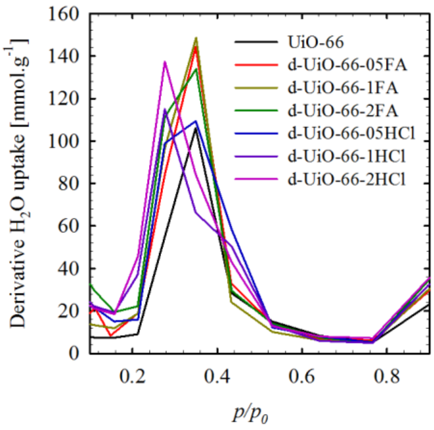

Figure S21 Derivative water adsorption isotherms at 298 K for UiO-66, d-UiO-66-aHCl and d-UiO-66-aFA (a = 05, 1, or 2, volume of additives used in the synthesis protocol).

S5 Density functional theory calculations

Static binding energies for CO_2 at zero Kelvin were calculated using the dispersion–corrected semi-empirical DFT-D2 method.[11] All calculations were performed using Vienna *ab* initio simulation package (VASP)[12,13] with a plane-wave energy cut-off of 500 eV and a Gamma-point mesh for sampling the Brillouin zone. The interactions between the core and valence electrons were described by the projector-augmented-wave (PAW) method, and the generalised gradient approximation (GGA) of Perdew-Burke-Ernzerhof (PBE)[14] was used to parameterize the exchange-correlation functional. As reported earlier in many studies, the strongest site for CO_2 adsorption in UiO-66 is the hydroxyl group located inside the tetrahedral cages.[24, 25] Thus, in this work a cluster model was built consisting of Zr metal-oxide with 12 linkers which was cleaved from the unit cell of UiO-66. The effect of missing linkers on the interaction energy of CO_2 was modelled, where one BDC linker was removed and replaced with formate, chloride and hydroxide to compensate the charge. The defective and perfect cluster model was modelled using a cell size of 35 x 35 x 35 Å in order to avoid interactions between repeated images. The initial location of the CO_2 in the periodic cell was obtained from the classical simulated annealing technique. In the simulated annealing method, the temperature was lowered successively allowing the gas molecule to reach a desirable configuration based on different moves such as rotate, translate and re-position with preset probabilities of occurrence. This process of heating and cooling the system was repeated in several heating cycles to find the local minima. Forty heating cycles were performed where the maximum temperature and the final temperature were 10^5 K and 100 K, respectively. Static binding energies (ΔE) at 0 K were calculated using the following expression;

$$\Delta E = E_{cluster+gas} - E_{cluster} - E_{gas}$$

where E_x refers, respectively, to the total energies of the cluster + gas complex, the cluster, and an isolated gas molecule.

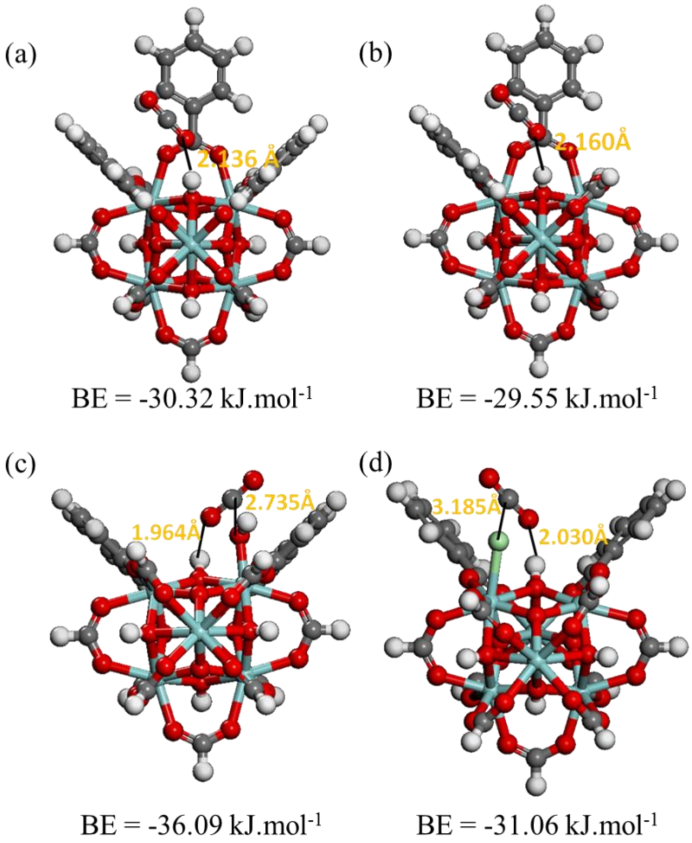

BE = -30.32 kJ.mol^{-1} BE = -29.55 kJ.mol^{-1}

BE = -36.09 kJ.mol^{-1} BE = -31.06 kJ.mol^{-1}

Figure S22 DFT - D2 optimised location and binding energy (B.E) of CO_2 for (a) perfect and defective cluster capped with (b) formate, (c) hydroxides and (d) chlorine group to compensate the charges.

S6 References

1. S. Luukkanen, M. Haukka, E. Eskelinen, T. A. Pakkanen, V. Lehtovuori, J. Kallioinen, P. Myllyperkiö and J. Korppi-Tommola, *Phys. Chem. Chem. Phys.*, 2001, **3**, 1992-1998.
2. M. J. Cliffe, W. Wan, X. Zou, P. A. Chater, A. K. Kleppe, M. G. Tucker, H. Wilhelm, N. P. Funnell, F.-X. Coudert and A. L. Goodwin, *Nat. Commun.*, 2014, **5**, 4176.
3. G. C. Shearer, S. Chavan, J. Ethiraj, J. G. Vitillo, S. Svelle, U. Olsbye, C. Lamberti, S. Bordiga and K. P. Lillerud, *Chem. Mater.*, 2014, **26**, 4068-4071.
4. M. J. Cliffe, J. A. Hill, C. A. Murray, F.-X. Coudert and A. L. Goodwin, *Phys. Chem. Chem. Phys.*, 2015, **17**, 11586-11592.
5. A. Schaate, P. Roy, A. Godt, J. Lippke, F. Waltz, M. Wiebcke and P. Behrens, *Chem.--Eur. J.*, 2011, **17**, 6643-6651.
6. F. Vermoortele, B. Bueken, G. Le Bars, B. Van de Voorde, M. Vandichel, K. Houthoofd, A. Vimont, M. Daturi, M. Waroquier, V. Van Speybroeck, C. Kirschhock and D. E. De Vos, *J. Am. Chem. Soc.*, 2013, **135**, 11465-11468.
7. M. Vandichel, J. Hajek, F. Vermoortele, M. Waroquier, D. E. De Vos and V. Van Speybroeck,

CrystEngComm, 2015, **17**, 395-406.

8. Y. Peng, G. Srinivas, C. E. Wilmer, I. Eryazici, R. Q. Snurr, J. T. Hupp, T. Yildirim and O. K. Farha, *Chem. Commun. (Cambridge, U. K.)*, 2013, **49**, 2992-2994.
9. J. M. Simmons, H. Wu, W. Zhou and T. Yildirim, *Energy Environ. Sci.*, 2011, **4**, 2177-2185.
10. P. D. C. Dietzel, V. Besikiotis and R. Blom, *J. Mater. Chem.*, 2009, **19**, 7362-7370.
11. G.-Q. Kong, Z.-D. Han, Y. He, S. Ou, W. Zhou, T. Yildirim, R. Krishna, C. Zou, B. Chen and C.-D. Wu, *Chem. - Eur. J.*, 2013, **19**, 14886-14894.
12. H. J. Park, D.-W. Lim, W. S. Yang, T.-R. Oh and M. P. Suh, *Chem. - Eur. J.*, 2011, **17**, 7251-7260, S7251/7251-S7251/7224.
13. O. K. Farha, A. Oezguer Yazaydin, I. Eryazici, C. D. Malliakas, B. G. Hauser, M. G. Kanatzidis, S.-B. T. Nguyen, R. Q. Snurr and J. T. Hupp, *Nat. Chem.*, 2010, **2**, 944-948.
14. P. Cui, Y.-G. Ma, H.-H. Li, B. Zhao, J.-R. Li, P. Cheng, P. B. Balbuena and H.-C. Zhou, *J. Am. Chem. Soc.*, 2012, **134**, 18892-18895.
15. J. L. C. Rowsell, E. C. Spencer, J. Eckert, J. A. K. Howard and O. M. Yaghi, *Science (Washington, DC, U. S.)*, 2005, **309**, 1350-1354.
16. H. Li, M. Eddaoudi, M. O'Keeffe and M. Yaghi, *Nature (Lond.)*, 1999, **402**, 276-279.
17. W. Lu, W. M. Verdegaal, J. Yu, P. B. Balbuena, H.-K. Jeong and H.-C. Zhou, *Energy Environ. Sci.*, 2013, **6**, 3559-3564.
18. A. R. Millward and O. M. Yaghi, *J. Am. Chem. Soc.*, 2005, **127**, 17998-17999.
19. U. Stoeck, S. Krause, V. Bon, I. Senkovska and S. Kaskel, *Chem. Commun. (Cambridge, U. K.)*, 2012, **48**, 10841-10843.
20. Z. R. Herm, J. A. Swisher, B. Smit, R. Krishna and J. R. Long, *J. Am. Chem. Soc.*, 2011, **133**, 5664-5667.
21. H. K. Chae, D. Y. Siberio-Perez, J. Kim, Y. B. Go, M. Eddaoudi, A. J. Matzger, M. O'Keeffe and O. M. Yaghi, *Nature (London, U. K.)*, 2004, **427**, 523-527.
22. S. M. Kuznicki, V. A. Bell, S. Nair, H. W. Hillhouse, R. M. Jacubinas, C. M. Braunbarth, B. H. Toby and M. Tsapatsis, *Nature (London, U. K.)*, 2001, **412**, 720-724.
23. Z. Zhang, Z.-Z. Yao, S. Xiang and B. Chen, *Energy Environ. Sci.*, 2014, **7**, 2868-2899.
24. H. Wu, Y. S. Chua, V. Krungleviciute, M. Tyagi, P. Chen, T. Yildirim and W. Zhou, *J. Am. Chem. Soc.*, 2013, **135**, 10525-10532.
25. H. Chevreau, W. Liang, G. J. Kearley, S. G. Duyker, D. M. D'Alessandro and V. K. Peterson, *J. Phys. Chem. C*, 2015, **119**, 6980-6987.